

0017-9310(94)00308-4

Augmentation of convective heat transfer by an effective utilization of droplet inertia

KOICHI HISHIDA, TATSUTO NAGAYASU and MASANOBU MAEDA

Department of Mechanical Engineering, Faculty of Science and Technology, Keio University,
3-14-1 Hiyoshi, Kohoku-ku, Yokohama 223, Japan

(Received 9 June 1994 and in final form 28 September 1994)

Abstract—Flow characteristics and heat transfer of a water droplets laden flow behind a backward-facing step have been experimentally and numerically investigated for the condition of isothermally heated dry wall. Two sizes of step heights were employed corresponding to $Re_H = 5.3 \times 10^3$, 1.1×10^4 . Numerical simulations were performed by a standard $k-\epsilon$ model for the gas phase and a Lagrangian stochastic model for the trajectories of droplets. The experimental and numerical results showed that large heat transfer enhancement existed downstream of the reattachment region and was correlated well with the ratio of time scale between an appropriate time scale of the turbulent flow and the relaxation time of droplet.

INTRODUCTION

In preparation for the persistent shortage of energy anticipated in the future, developments of the alternative energy source and in techniques for recovery of waste heat are of increasing important. Generally, the qualities of such alternative energy are relatively low, so that high performance heat exchangers even under the small temperature difference are necessary for an effective utilization of energy. One way to realize such heat transfer devices is to employ a liquid particle laden flow as the operational fluid. The prominent effectiveness of air–water droplets flow on increasing heat transfer was proved by an experimental study of a laminar boundary layer flow [1], which indicated that the heat transfer coefficient became several times larger than that of the single-phase flow with the addition of latent heat due to the evaporation of the droplets near the heated wall. Although the potential of that flow for augmenting heat transfer is very high, the system does not have the sufficient performance in many flows, since droplets flow passively in the working fluid and are ejected by the displacement effect from the boundary layer. Consequently, if one could control the motion of the droplets actively and attach these to the heated flat plate, an effective and large enhancement of the heat transfer can be expected in an air–water droplet flow.

The motion of the particle has been investigated by many investigators. Chein and Chung [2, 3] performed numerical studies of particle dispersion in turbulent shear flows taking into account the effects of the large scale eddies. In these works, they pointed out that the Stokes number, St , which was defined by the ratio of the time scale of particle motion and of the large scale fluid motion, correlated to the phenomena of the particle dispersion. More recently, accurate exper-

iments have been available with the improvement of Laser Doppler Anemometry. Hishida *et al.* [4] examined the particle dispersion in a turbulent mixing layer. The result indicated that the particles dispersion coefficients became larger than the eddy diffusivity of the gas phase in a certain range of Stokes number. Because the particle motions are dominated by interactions with the large-scale structures of turbulent flows, actively varying the large scales implies that the particle motion can be controlled. As a consequence, the heat transfer in an air–water droplet flow would be increased effectively by the use of such controlling mechanisms for liquid particles.

A flow field which contains the large scale structure is the flow behind a backward-facing step. Single-phase flow characteristics in this geometry were studied in many excellent detailed works. Bradshaw and Wong [5] reported an experiments on the low-speed flow downstream of steps and fences which were used to demonstrate the complicated nature of the flow in the reattachment region and its effect on the slow non-monotonic return of the shear layer to the ordinary boundary layer. Eaton and Johnston [6] reported series of experiments that the spanwise vortices existed and were the dominant structure in the shear layer even when the separating boundary was turbulent. From these works it became clear that the turbulent structure and time scale in the separated shear layer depend on step height. Therefore, it is considered to be able to control the particle motion by changing Stokes number depending on the step height.

The flow characteristics and heat transfer of gas–solid two-phase flow behind a backward-facing step were studied by the author's group [7]. That work focused on the turbulence modification such as attenuation or enhancement of turbulence and the heat transfer in the recalculation region to develop a

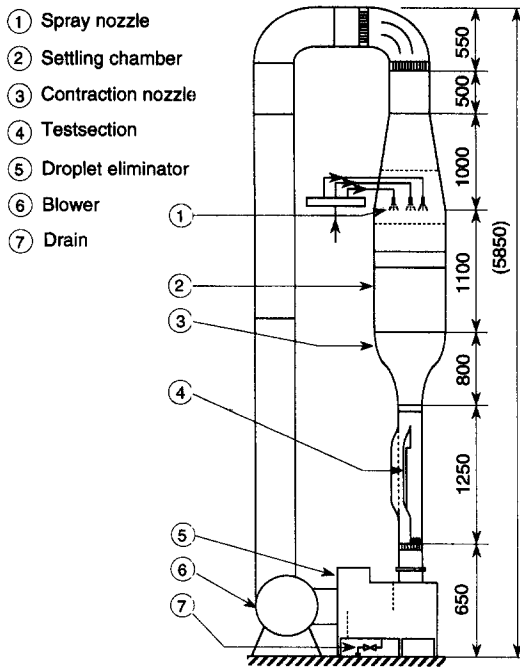


Fig. 1(a). Wind tunnel.

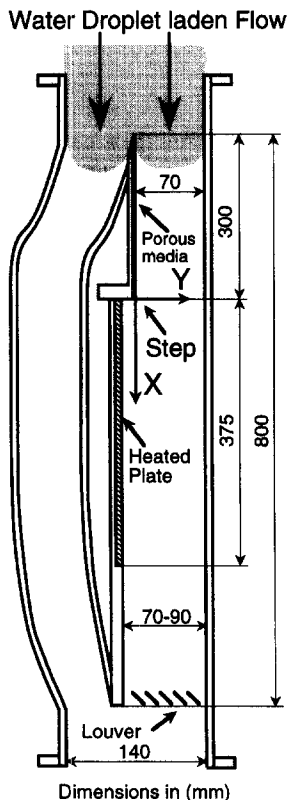


Fig. 1(b). Test section schematic.

opment. The cross section of the heating section could expand from 70 mm \times 210 mm to 90 mm \times 210 mm by changing the step height, where the width of the test section was 210 mm. The droplet mass flow rate

was measured by isokinetic sampling as same as the previous study [1]. The cross sectional distribution of mass flow rate at the inlet of the test section was almost uniform within 10% based on the overall average value.

The heated flat plate had multilayer construction which contained a copper plate, main heater, back-up heater, insulation, aluminum plate and a thin air layer to avoid heat loss by conduction. The main heater was divided into 12 sections in the flow direction, and each section was heated individually by controlling the electric power supply. The temperature of each heater was monitored to keep the isothermal surface by copper-constantan thermocouples of 80 μ m in diameter which were buried just under the wall. Local heat transfer coefficients h were obtained from local heat flux divided by the temperature difference between wall and dry bulb temperatures in free stream.

Flow measurement

The Phase Doppler Anemometer (PDA) system schematically shown in Fig. 2 was employed for the measurements of the droplet size, droplet mass flux, and X and Y components of velocity. The transmitting optics consisted of a 2 W Ar-ion laser source, beam splitters, double Bragg cells for measuring the reverse flow, and the transmitting probe which was linked by optical fiber cables. Two pairs of beams with 26 mm parallel distance were focused by a lens of 300 mm focal length. The measuring volume was approximately 0.2 mm \times 0.2 mm \times 0.5 mm. The receiving optics of the PDA system had four channels, one channel was for the transverse velocity, and three channels were for the streamwise velocity and phase detection. The diameter of droplet was evaluated from the phase difference in the PDA system. The signal processor has been developed by the authors' group [9]. The scattered light from the droplets was detected by photo multipliers and digitized in a fast A/D converter at 50 MHz and then transferred to the FFT-type signal processing unit. For real time measurements, Digital Signal Processors (DSP) were installed in the processing unit to achieve high speed calculation of FFT and digital filters. Mean velocity and its fluctuation, droplet size distribution and droplet mass flux were evaluated from more than 5000 data.

Experimental condition

Two steps, with $H = 10$ mm and 20 mm, were used to vary the turbulent structure in the separated shear layer. The free stream velocity just upstream of the separation point was fixed to 10.0 m s^{-1} , which corresponds to step-height Reynolds numbers of 5.3×10^3 and 1.1×10^4 , respectively. The boundary layer state at the separation point is one of the important factors for the behaviour of the flow field, so that the boundary layer state should be clear in the experiments. Figure 3 shows the streamwise mean velocity and turbulence intensity profiles just upstream of the

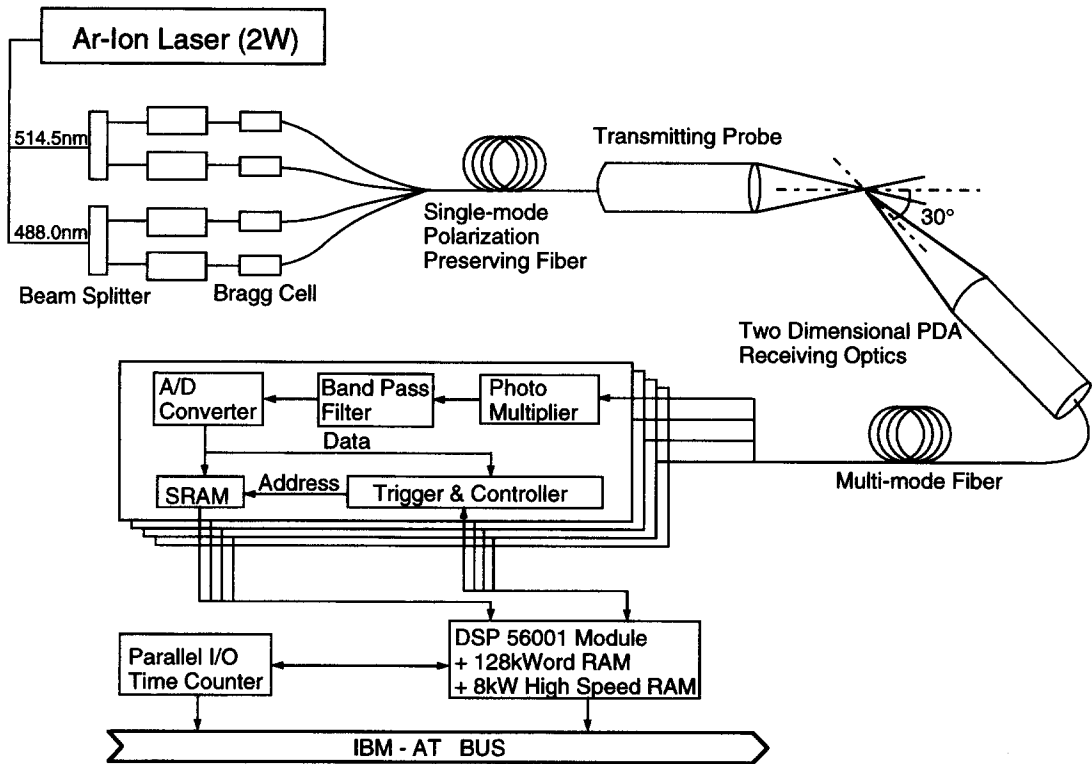


Fig. 2. Schematic view of the measuring system.

separation point ($X = -10$ mm). The mean velocity profiles in the present experiment agreed with that of Klebanoff [10]. The streamwise turbulence intensity was a little bit larger than Klebanoff's data due to the roughness of the wall surface made by porous metal in the boundary layer development section. These profiles clearly showed that the boundary layer was turbulent at the separation point. The mass loading ratio of water droplets was set at 4.1% to realize a dry heated wall condition which was experimentally con-

firmed. Figure 4 illustrates the droplet size distribution in the free stream which was fitted with the Rosin-Rammler formula. The arithmetic mean diameter was about $60 \mu\text{m}$. The experimental conditions and parameters of this work are summarized in Table 1.

Uncertainty

The uncertainty of every value was estimated by the method of "Root Sum Square Methods" [11]. This

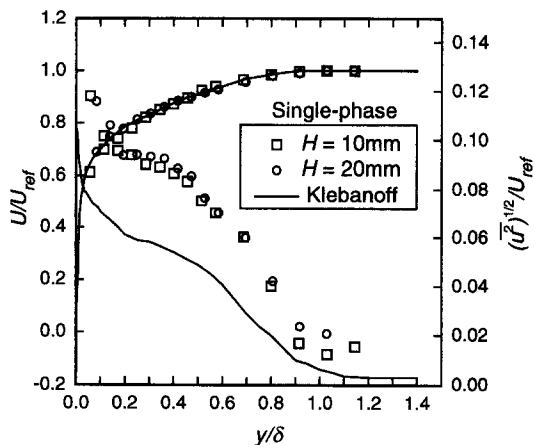


Fig. 3. Streamwise mean velocity and intensity in single phase ($X = -10$ mm).

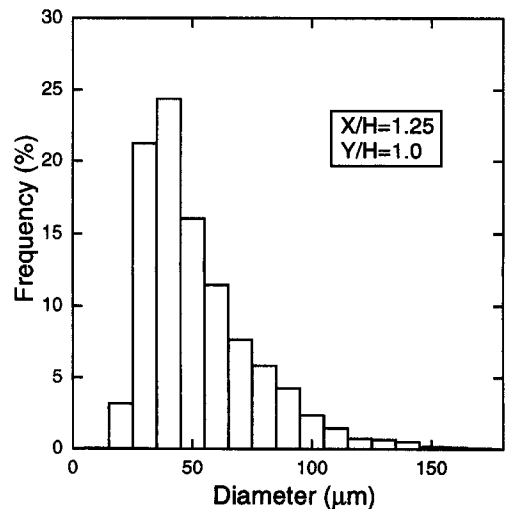


Fig. 4. Distribution of droplet size in free stream.

Table 1. Experimental conditions

| | | |
|-------------------------------------|----------------|-------------------------------|
| Step height | H | 10, 20 [mm] |
| Expansion ratio | ER | 1.14, 1.29 |
| Wall temperature | T_w | 35, 50, 65, 80, 100, 130 [°C] |
| Free stream temperature | $T_{ad\infty}$ | 15–25 [°C] |
| Arithmetic mean diameter of droplet | D_p | 60 [μm] |
| Relative humidity of air | ϕ | 95.0 [%] |
| Mass loading ratio | M | 4.1 [%] |

Table 2. Measurement uncertainty

| Value | Uncertainty [%] |
|---------------------------------------|-----------------|
| U/U_{ref} | 1.3 |
| $(\langle u^2 \rangle)^{1/2}/U_{ref}$ | 1.1 |
| V/U_{ref} | 0.8 |
| $(\langle v^2 \rangle)^{1/2}/U_{ref}$ | 5.2 |
| Sth/Sth_{max} | 8.7 |

method estimates a 95% confidence interval for each value. The results of uncertainty analysis are shown in Table 2.

Numerical simulation

Governing equations and turbulence model for gas phase. The flow was treated as a steady-state, incompressible, two-dimensional flow of uniform fluid properties. The mean flow was described with the continuity equation and momentum equation. Recently, several kinds of turbulence models have been developed for accurate numerical prediction. In the present study, the standard high Reynolds number $k-\varepsilon$ model [12] was employed here to represent the turbulence. It is known that the standard $k-\varepsilon$ model predicts poorly in a backward-facing step flow, but it is still widely used for industrial purposes, and it is considered to be appropriate with a view to helping the understanding the mechanism of heat transfer enhancement in two-phase flows. The governing equations are given as

$$\frac{\partial U_i}{\partial X_i} = 0 \quad (1)$$

$$\frac{DU_i}{Dt} = -\frac{1}{\rho} \frac{\partial P}{\partial X_i} + \frac{\partial}{\partial X_j} \left(\frac{\mu}{\rho} \frac{\partial U_i}{\partial X_j} - \overline{u_i u_j} \right) \quad (2)$$

$$-\overline{u_i u_j} = \frac{\mu_t}{\rho} \left(\frac{\partial U_i}{\partial X_j} + \frac{\partial U_j}{\partial X_i} \right) - \frac{2}{3} \delta_{ij} k \quad (3)$$

$$\mu_t = C_\mu \rho k^2 / \varepsilon \quad (4)$$

$$\frac{Dk}{Dt} = \frac{\partial}{\partial X_j} \left\{ \left(\frac{\mu}{\rho} + \frac{\mu_t}{\rho \sigma_k} \right) \frac{\partial k}{\partial X_j} \right\} - \overline{u_i u_j} \frac{\partial U_i}{\partial X_j} - \varepsilon \quad (5)$$

$$\frac{D\varepsilon}{Dt} = \frac{\partial}{\partial X_j} \left\{ \left(\frac{\mu}{\rho} + \frac{\mu_t}{\rho \sigma_\varepsilon} \right) \frac{\partial \varepsilon}{\partial X_j} \right\} - C_{\varepsilon 1} \frac{\varepsilon}{k} \overline{u_i u_j} \frac{\partial U_i}{\partial X_j} - C_{\varepsilon 2} \frac{\varepsilon^2}{k} \quad (6)$$

where $C_\mu = 0.09$, $C_{\varepsilon 1} = 1.44$, $C_{\varepsilon 2} = 1.92$, $\sigma_k = 1.0$, $\sigma_\varepsilon = 1.3$.

For the temperature, the enthalpy transport equation was solved as a passive scalar, and the turbulent heat flux was expressed using a turbulent Prandtl number. The governing equations for the temperature are given as

$$\frac{D\Phi}{Dt} = \frac{\partial}{\partial X_j} \left(\frac{\mu}{\rho Pr_t} \frac{\partial \Phi}{\partial X_j} - \overline{u_j \Phi} \right) \quad (7)$$

$$-\overline{u_j \Phi} = \frac{\mu_t}{\rho Pr_t} \frac{\partial \Phi}{\partial X_j} \quad (8)$$

The wall function method [12], bridging the viscous near-wall zone with the outer flow using empirical assumptions, was used to specify wall boundary conditions for the velocity and temperature fields. The turbulent Prandtl number Pr_t was set at 0.85 as given in ref. [13].

Numerical solutions of these partial differential equations were obtained using a finite volume method with collocated (non-staggered) variable arrangement. The pressure and mean velocity fields were coupled with the SIMPLE algorithm by Patankar and Spalding [14]. The convective terms in the momentum equations were discretized with the third-order upwind-differencing scheme QUICK by Leonard [15] to avoid effects of numerical diffusion. The convergence criterion was achieved for all variables less than 10^{-4} where the absolute residual sums were normalized by the inlet fluxes.

Governing equations for dispersed phase. Generally, calculations for the particles phase are classified between two types, one is the Eulerian approach and the other is the Lagrangian approach. In the present work, the Lagrangian approach was employed for the prediction of droplet trajectories. The experimental mass loading ratio of droplets to gas flow was small enough to assume no turbulence modification by the existence of the droplets. So the calculation for the droplets was performed after solving for the gas phase (“one-way coupling method”).

Particle trajectories were calculated in the flow field of single phase calculated by the standard $k-\varepsilon$ model. The droplets introduced in the input plane of the solution domain have the same arithmetic mean diameter of droplets as in the present experiments. The governing equation of the droplets is the equation of

motion of a spherical particle. The forces acting on the droplet are the viscous and pressure drag, force due to fluid pressure gradient and viscous stresses, inertia force of added mass, viscous force due to unsteady relative acceleration, and the buoyancy (or gravity) force. In these forces, the drag and gravity play the most important role for the droplet motion. A steep velocity gradient would be expected to exist in the separated shear layer behind the step. Therefore, the Saffman drift force [16] should be included in the equation for motion. With these considerations, the equation of motion becomes

$$m_p \frac{d\mathbf{V}_p}{dt} = -\frac{3}{4} \frac{m_p}{d_p} \frac{\rho_f}{\rho_p} C_D (\mathbf{V}_p - \mathbf{U}_f) |\mathbf{V}_p - \mathbf{U}_f| + m_p \left(1 - \frac{\rho_f}{\rho_p}\right) \mathbf{g} + \mathbf{F}_L \quad (9)$$

Drag coefficients [17]

$$C_D = \frac{24}{Re_p} (1 + 0.15 Re_p^{0.687}) \quad Re_p \leq 200$$

$$Re_p = \frac{|\mathbf{V}_p - \mathbf{U}_f| d_p}{\nu} \quad (10)$$

Saffman drift force

$$F_{L1} = 0$$

$$F_{L2} = m_p \frac{6C_s(\rho_f \mu)^{0.5}}{\pi d_p} \left| \frac{dU_1}{dX_2} \right|^{0.5} (\mathbf{U}_f - \mathbf{V}_p). \quad (11)$$

The equation of motion for the particle includes an instantaneous velocity of the fluid at the particle position. So it is required to introduce the instantaneous velocity of the fluid from the mean velocity and turbulent kinetic energy. One possible way is the random sampling from the turbulent kinetic energy, but it is impossible to reproduce the actual flow field because the standard model does not allow the correlation between streamwise and transverse velocities. Thus, a two-dimensional probability density model [18] was applied to introduce the instantaneous velocity field where the Reynolds shear stress existed. This model induces the instantaneous velocity calculated stochastically from mean velocities and turbulent kinetic energy, and ensemble averaged quantities of the flow field induced by this model are exactly the same quantities which are calculated in the single-phase flow prediction. In this work, the velocity field of droplets were evaluated statistically from the trajectories of droplets calculated with the procedure described above.

Estimation of Reynolds stress

The stochastic model described above requires the instantaneous velocity of the fluid, but the turbulent kinetic energy in each direction is unknown. The turbulent flow field considered in this work is a flow behind a backward-facing step and has a strong anisotropy. The standard high Reynolds number $k-\varepsilon$

model applied in the present work is based on the isotropic Boussinesq approximation, so that it yields highly inaccurate predictions for the Reynolds stress differences between the streamwise and transverse components. Therefore, the algebraic relation by Rodi [19] was adopted for recalculating the Reynolds stresses. In this method, the Reynolds stresses were estimated from the converged results of the turbulent kinetic energy and its dissipation which was simulated by the standard high Reynolds number $k-\varepsilon$ model, and this relation is given as

$$P_{ij} = \left\{ v_i \left(\frac{\partial U_i}{\partial X_k} + \frac{\partial U_k}{\partial X_i} \right) - \frac{2}{3} k \delta_{ik} \right\} \frac{\partial U_j}{\partial X_k} + \left\{ v_i \left(\frac{\partial U_j}{\partial X_k} + \frac{\partial U_k}{\partial X_j} \right) - \frac{2}{3} k \delta_{jk} \right\} \frac{\partial U_i}{\partial X_k} \quad (12)$$

$$P = \frac{1}{2} P_{ii} = -\overline{u_k u_l} \frac{\partial U_k}{\partial X_l} \quad (13)$$

$$\overline{u_i u_j} = k \left\{ \frac{2}{3} \delta_{ij} + \frac{1-\gamma}{C_1} \frac{P_{ij}/\varepsilon - 2/3 \delta_{ij} \cdot P/\varepsilon}{1 + 1/C_1 (P/\varepsilon - 1)} \right\}$$

$$C_1 = 1.5, \quad \gamma = 0.6. \quad (14)$$

Numerical prediction of droplet motion was performed with the mean velocity field which was obtained by standard $k-\varepsilon$ model and the Reynolds stresses which were estimated by the method described above. In a droplet laden flow, heat transfer is increased by the sensible and the latent heat of the droplets attached to the heated flat plate. The latent heat due to the evaporation of droplets mainly contributes to enhancement of heat transfer, that is, a variation of droplet temperature in the thermal boundary layer could be neglected. Therefore, droplet motion is only solved before attachment to the heated wall. We assume that droplets attached to the heated wall instantaneously evaporate on the heated wall. The numerical results of heat flux from the heating wall were obtained by the summation of heat flux to single-phase flow and sensible and latent heat of droplets attached to the heated flat plate.

RESULTS AND DISCUSSION

Mean velocity profiles

The streamwise mean velocity profiles of both phases at different downstream locations from the step are presented for $H = 20$ mm in Fig. 5(a) and for $H = 10$ mm in Fig. 5(b). The experimental results show the same typical features of the single-phase flow described in the previous work [20]. From the results of the two-phase flow, it is observed that there was a region immediately downstream of the step in which droplets were not observed. In addition, the droplet velocities were larger than those of the air phase in the separated shear layer, and this velocity difference (slip velocity) in the $H = 10$ mm case was larger than the $H = 20$ mm case. These results indicate that the

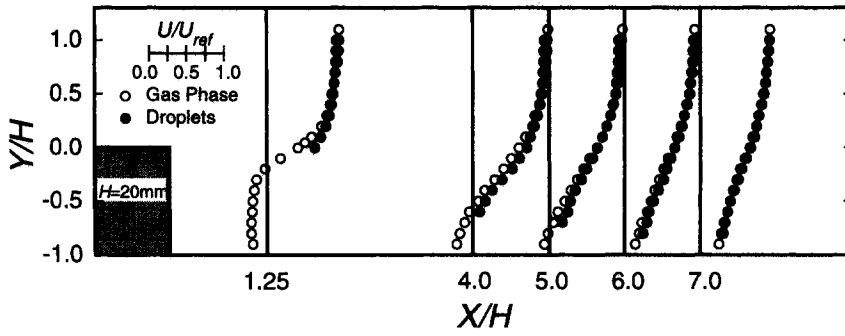


Fig. 5(a). Mean velocity profiles of gas and droplets for $H = 20$ mm.

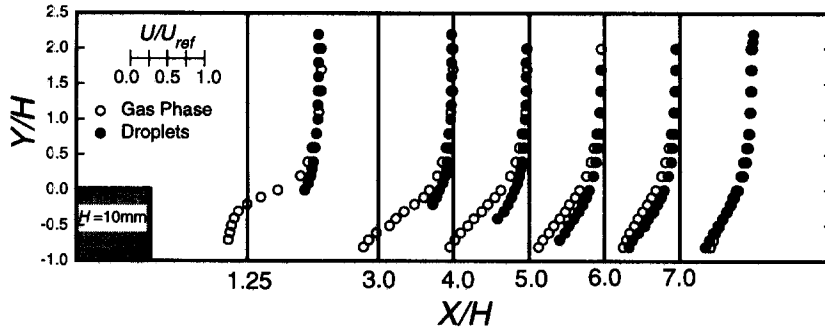


Fig. 5(b). Mean velocity profiles of gas and droplets for $H = 10$ mm.

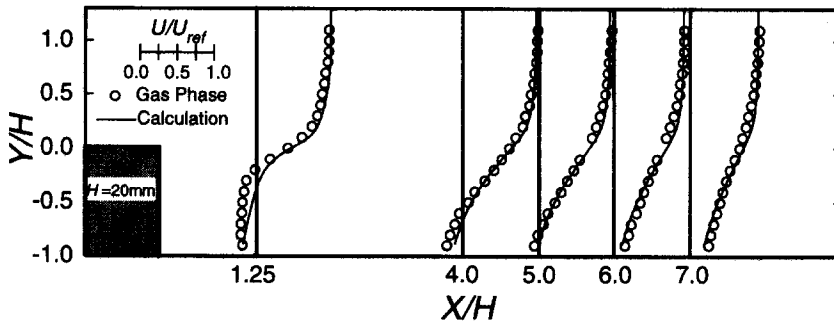


Fig. 5(c). Mean velocity profiles of gas for $H = 20$ mm.

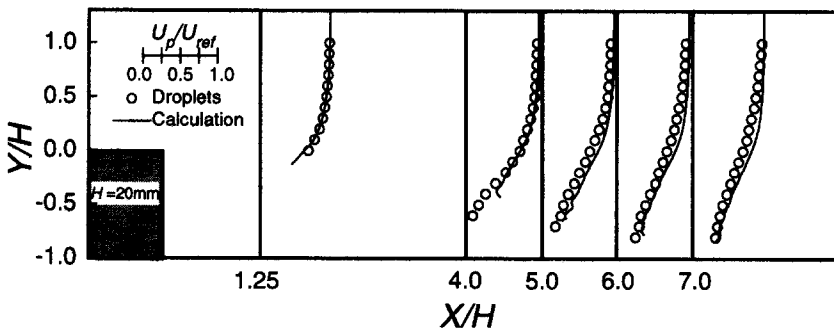


Fig. 5(d). Mean velocity profiles of droplets for $H = 20$ mm.

droplets follow insufficiently the single-phase flow. In particular, the difference of slip velocity between the two step heights is interesting and important to understand the interaction between droplets and the air-phase flow in the two-phase flow. This discussion will

be described later in the section on local Stokes number profiles. The comparison between experimental and numerical results in the single-phase flow is shown in Fig. 5(c). The standard high Reynolds number $k-\epsilon$ model predicted a shorter reattachment length. This

Table 3. Reattachment length

| Step height | 10 mm | 20 mm |
|-------------|-------|-------|
| Experiment | 6.00H | 6.13H |
| Calculation | 4.21H | 5.39H |

is one of the weaknesses which was pointed out by many investigators. The most important dependent parameter characterizing the flow behind a backward-facing step is the reattachment length, so that the reattachment lengths obtained from experiments and numerical prediction should be examined to understand better the flow field. The reattachment lengths of experiments and numerical calculation are summarized in Table 3. In the experiments, the reattachment lengths were calculated from the extra-

polation of the dividing stream line, and normal interpolation was used to obtain the reattachment length in the numerical simulation. Figure 5(d) shows the comparison between results of experiments and simulation of the droplet mean velocities. Numerical simulation predicted the droplets free zone which was observed in the experimental results. There is a small difference between experiments and numerical simulations about the droplet-free zone which gives a later attachment of the droplets in the simulation than that in the experiments.

Turbulence properties

The two-component turbulent kinetic energy [$(\langle u^2 \rangle + \langle v^2 \rangle)/2$] profiles in single-phase flow of $H = 20$ mm are shown in Fig. 6(a). The simulated two-component turbulent kinetic energy profiles were

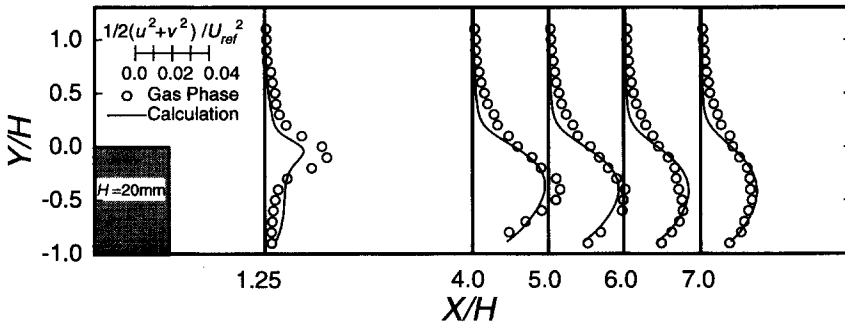


Fig. 6(a). Turbulent kinetic energy of gas phase for $H = 20$ mm.

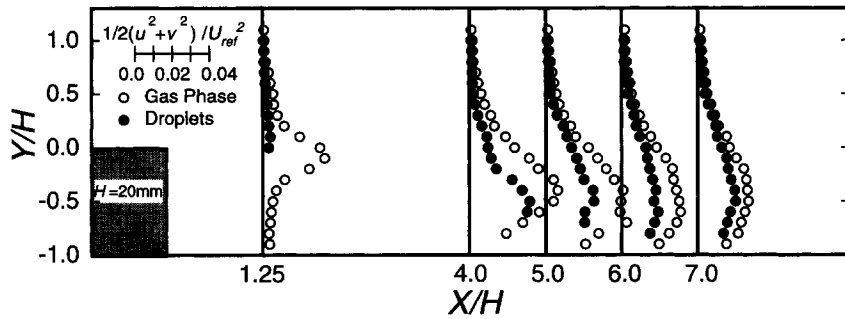


Fig. 6(b). Velocity fluctuation of gas and droplets for $H = 20$ mm.

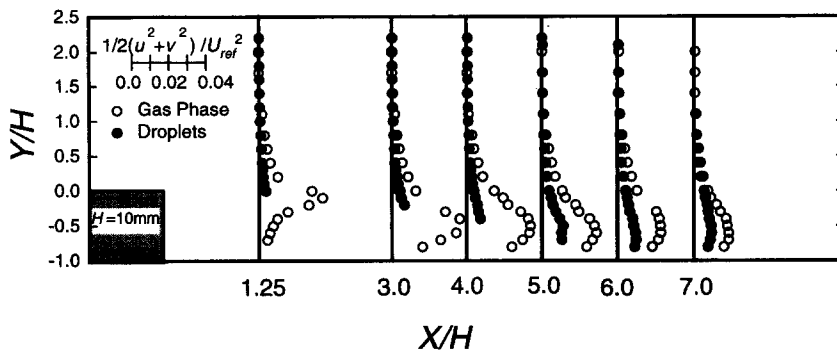


Fig. 6(c). Velocity fluctuation of gas and droplets for $H = 10$ mm.

calculated by the summation of normal Reynolds stresses obtained from the Reynolds stresses estimation described above. The measured turbulent kinetic energy demonstrated the same tendency of the previous works [20, 21], and numerical results showed the good agreement with the experimental data. The maximum turbulent kinetic energy was located near the dividing stream line, and took a peak value at the distance of one to two step heights upstream from reattachment, and decreased rapidly near the reattachment. The velocity fluctuation of the droplets and the turbulent kinetic energy of the gas phase for $H = 20$ mm are represented in Fig. 6(b), and also Fig. 6(c) shows the case of $H = 10$ mm. The same features are observed in both step heights. A higher level of kinetic energy is noted for $H = 20$ mm case caused by the higher rate of production from the more distorted mean velocity profile due to the larger expansion ratio. The maximum velocity fluctuation of droplets was smaller than that of the gas phase, but increased along the dividing stream line as for the gas phase flow. This result indicates that the droplets are dispersed by the large eddies in the separated shear layer.

Profiles of local Stokes number

It was reported by authors' group [4, 22] that the interaction between droplet and fluid is well correlated with the Stokes number St . The definition of the Stokes number is written as follows

$$St = \frac{\tau_p}{\tau_r} \quad (15)$$

where τ_r is an appropriate mean of turbulent time-scale of the flow field and τ_p is a particle relaxation time given as

$$\tau_p = \frac{\rho_p \cdot d_p^2}{18\mu_a} \quad (16)$$

The Stokes number qualifies the ability of the droplet to follow a fluid motion. If $St \ll 1$, the droplet follows the corresponding characteristic time-scale of the fluid, while if $St \gg 1$ the particle is not affected. For describing the turbulent motion, it is convenient to decompose the instantaneous motions into mean values and fluctuations. The important features of the flow behind a backward-facing step are: (i) the curvature effect of the mean stream lines in single-phase flow, (ii) the decreasing velocity in the free stream due to the sudden expansion and (iii) the large-eddy structure in a separated shear layer, as pointed out by Hardalupas *et al.* [8] for the round sudden-expansion flow. So it is required that the τ_r can represent these three characteristics. The mean flow features, namely the curvature effect and the decreasing velocity, can be estimated by the equations below:

the curvature effect

$$St_c = \frac{\tau_p}{\tau_r} = \frac{\tau_p}{r/U_{cur}} \quad (17)$$

Table 4. Stokes number for mean motion

| Step height | 10 mm | 20 mm |
|-------------|-------|-------|
| St_c | 0.54 | 0.25 |
| St_d | 0.15 | 0.07 |

the decreasing velocity in free stream

$$St_d = \frac{\tau_p}{\tau_r} = \frac{\tau_p}{1/(\partial U/\partial X)} = \frac{\tau_p}{X_r/(U_{ref,at X=0} - U_{ref,at X=X_r})} \quad (18)$$

where r is the representative value for the curvature of the mean stream line. r was estimated by the radius of arc which fitted the dividing stream line. These Stokes numbers which include particle relaxation time of arithmetic diameter in these experiments are shown in Table 4. St_d is very small as compared with unity. Therefore, the droplets can follow the mean fluid flow of decreasing velocity associated with the sudden expansion. In contrast, St_c are less than unity, but they are not small enough to allow the droplets to follow the fluid motion along the curved mean stream lines. Especially in the case of $H = 10$ mm, the value of St_c is 0.54, so that one can expect that the droplets behave differently from the air motion because of its centrifugal force acting on the droplets. This discussion can be clarified by a comparison with the mean streamwise velocity profiles of $H = 20$ mm and $H = 10$ mm shown in Figs. 5(a) and (b). The slip velocities, and the velocity differences between droplets and single-phase flow, are negligible far from the wall (free stream side) in both step heights, but they have significant values around the separated shear layer. In addition, the slip velocities around the separated shear layer for the $H = 10$ mm case are larger than that for $H = 20$ mm. These findings show clearly that the above discussion is reasonable.

The turbulent Stokes number includes the τ_r which represents turbulent motion, namely, energy containing eddy in the separated shear layer, and also is defined by the length scale and velocity scale of that eddy. The large eddy structure has the same size as the separated shear layer thickness, so the shear layer thickness was chosen as the length scale. The shear layer thickness was obtained by the treatment by Johnston [23], and its description is sketched in Fig. 7. The root mean square value of turbulent kinetic energy was employed in the velocity scale in order to express the strength of the energy containing eddies. The turbulent Stokes number was evaluated using these scales as follows:

$$St_c = \frac{\tau_p}{\tau_r} = \frac{\tau_p}{\delta/\sqrt{k}} \quad (19)$$

Turbulent Stokes number profiles are shown in Fig. 8. Droplet size distribution, as shown in Fig. 4, is continuous, but droplet diameters of 30, 60 and 90 μm were chosen to estimate the relaxation times.

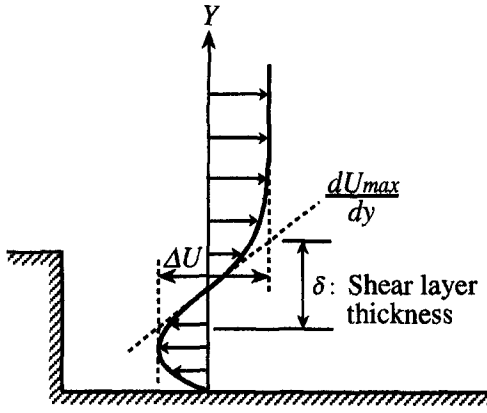


Fig. 7. Shear layer thickness.

St_c for $H = 20$ mm and droplet of $60 \mu\text{m}$ became around unity downstream of $X/H = 4$. When the Stokes number is around unity, the droplets disperse more than the fluid (this phenomena is called “over shoot”). Therefore, droplets of that size dispersed much more than the other sizes of droplet in the separated shear layer. Droplets could enter around the recirculating region only by the turbulent motion because there is no convection across the dividing stream line. It is clear from Fig. 8 that only small particles with diameters less than at least $30 \mu\text{m}$ could follow the turbulent motion and enter the recirculating region.

Distributions of droplet size and droplet mass flux

Figure 9(a) shows the local size distributions of droplets at $X/H = 6$ when droplets traverse toward the Y direction and (b) shows the local size distributions at $Y/H = -0.5$ when droplets traverse toward the streamwise direction. (a) shows that only small droplets can enter the recirculating region. This can be indicated by the turbulent Stokes number

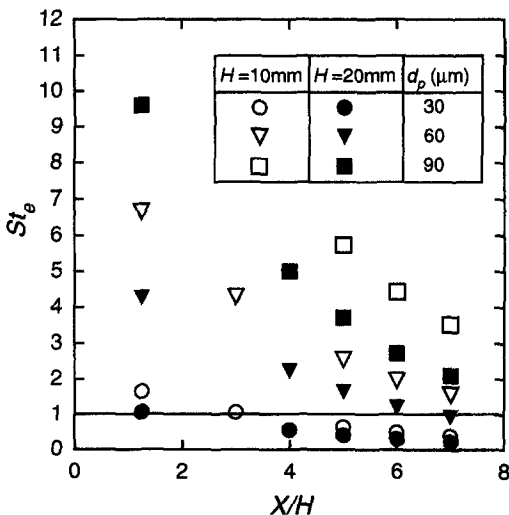


Fig. 8. Turbulent Stokes number profiles.

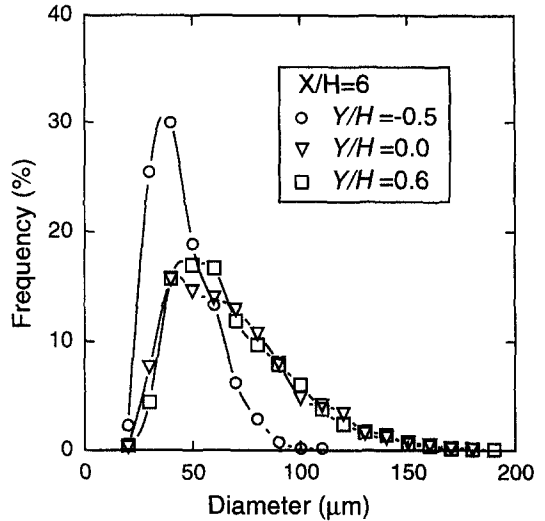


Fig. 9(a). Local size distributions of droplets ($X/H = 6$).

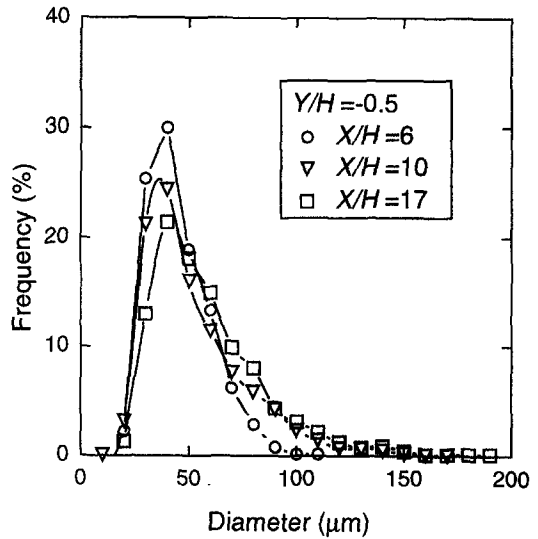


Fig. 9(b). Local size distributions of droplets ($Y/H = -0.5$).

defined previously because particles can penetrate the recirculating region only by turbulent motion. It is observed that the mean droplet size increases downstream in Fig. 9(b). This can be explained by the magnitudes of St_c shown previously, which suggest that large droplets barely follow the air-phase because of their strong inertia.

Figure 10(a) shows the streamwise droplet mass flux profiles for $H = 20$ mm. Mass fluxes were evaluated from the product of the number of droplets per unit time which passed through the measuring volume of the PDA system and the mass of each droplet. These mass fluxes were normalized by the mass flux in free stream at the separation point. It is evident that the mass flux is very small in the recirculating region. Numerical results show that the mass flux is larger than in the experiment around the reattachment region, but they present the same trend as the exper-

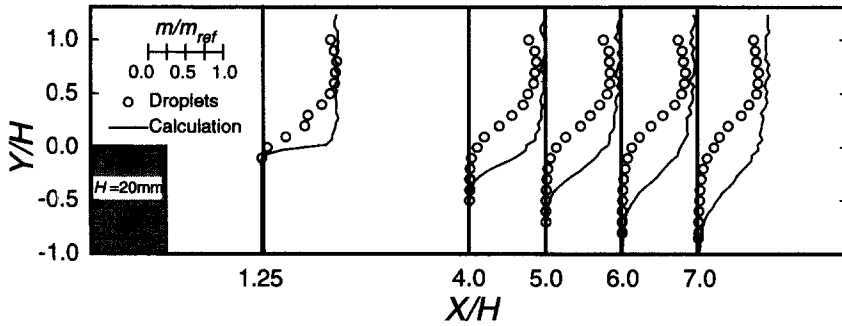


Fig. 10(a). Profiles of droplet mass flux for $H = 20$ mm.

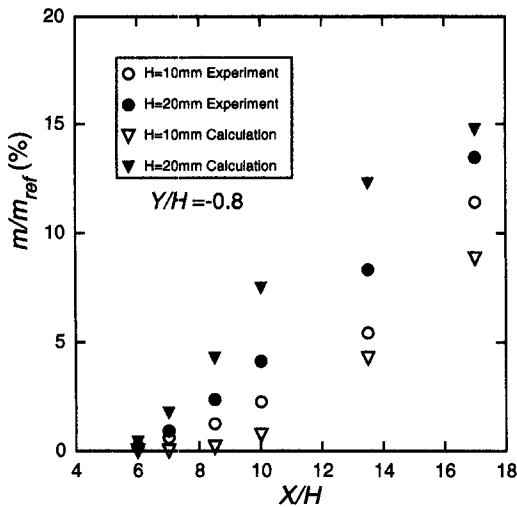


Fig. 10(b). Mass flux of droplet near the wall for $H = 20$ mm.

imental results. The mass of the droplets which attach to the heated flat plate is of significance in increasing the heat transfer. The mass flux to the adjacent wall is presented in Fig. 10(b). Mass fluxes increase downstream in both experimental and numerical results, so that the mass of attached droplets should increase.

Heat transfer characteristics

Heat transfer in single-phase flow. The Stanton number profiles of single-phase flow are shown in Fig. 11. The Stanton number St_h was defined as

$$St_h = h / (\rho_f C_{pf} U_{ref}), \quad (20)$$

where ρ_f is density of air and C_{pf} is specific heat of air in single and two-phase flow. Stanton numbers are plotted versus normalized distances of X^* based on reattachment lengths for each condition as indicated in Table 3. These results almost agree with the previous data [21, 24] when Stanton numbers were normalized by the maximum value of each condition and plotted to X^* to prevent any dependence on the step Reynolds number. The Stanton number profiles from the numerical simulation give a smaller maximum value in both cases, but the tendency agrees with the experimental data. The location of the maximum

Stanton number slightly shifts upstream because the reattachment length obtained from the prediction is shorter than that of the experiment in both cases. A boundary condition of the heated flat plate was basically given by the wall function of Launder and Spalding [12]. The wall function requires the turbulent kinetic energy at the adjacent grid point from the wall, but, when the convection strongly affects the heat transfer, using the turbulent kinetic energy at the grid point which is next to the adjacent grid point gives an improved heat transfer prediction [25].

Heat transfer in two-phase flow. Figures 12(a) and (b) present the Stanton number profiles along streamwise length in two-phase flow, where Stanton numbers in single- and two-phase flows are normalized by the maximum value in the single-phase flow. Large enhancement of heat transfer was observed downstream following the reattachment region for every condition of wall temperature. Especially, heat transfer for $H = 20$ mm is more augmented than that for $H = 10$ mm just downstream of reattachment. The results obtained from the numerical prediction, shown in Fig. 13, have the same trend as the experimental results though the calculation predicts that the location where the heat transfer starts to increase

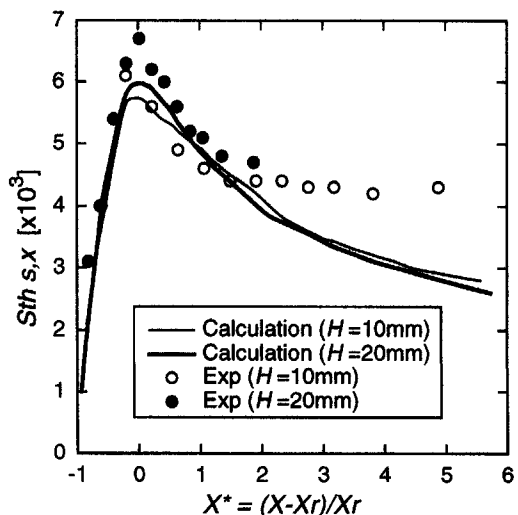


Fig. 11. Stanton number profiles in single-phase flow.

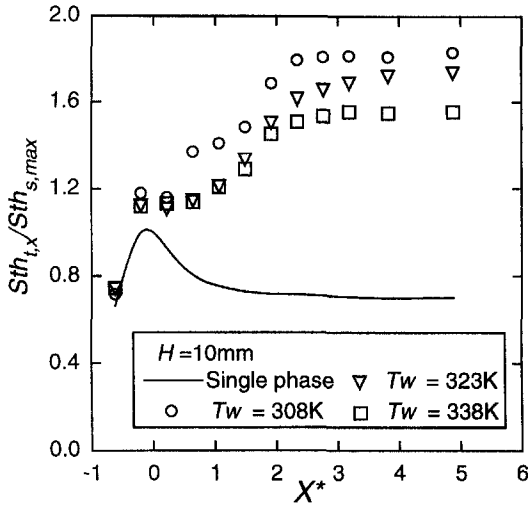


Fig. 12(a). Stanton number profiles in two-phase flow for $H = 10$ mm.

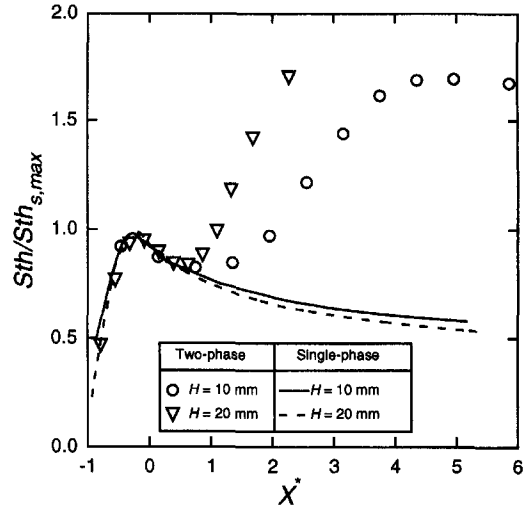


Fig. 13. Stanton number profiles in two-phase flow for calculation.

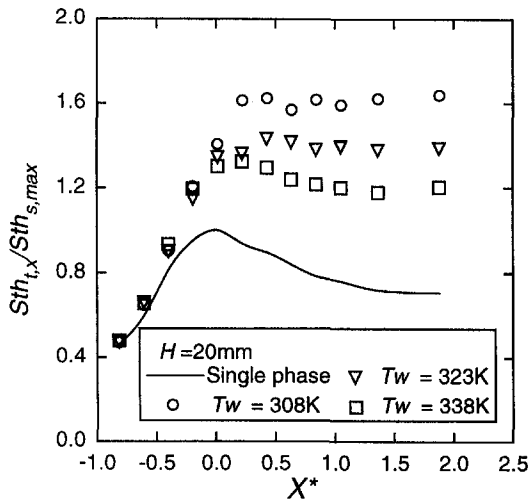


Fig. 12(b). Stanton number profiles in two-phase flow for $H = 20$ mm.

the mass flux of the droplets attached on the heated flat plate.

For the purpose of a better consideration of the heat transfer enhancement in two-phase flow, the ratio of local Stanton number in two-phase flow to that of the single-phase flow for X^* was presented in Fig. 14. It is observed that the heat transfer increases downstream of the reattachment region and slightly depends on the Reynolds number based on the step height. The increase in Stanton number ratio for $H = 20$ mm is slightly larger than that for $H = 10$ mm just after the reattachment. This result is directly connected to the increase of the mass flux of the droplets attached to the heated plate, and it agrees with the result of mass flux profiles as shown in Fig. 10(b). This result can be explained by the different turbulent structure in the separated shear layer in the two step heights, namely, the droplets in the flow with $H = 20$ mm are dispersed more than that for $H = 10$ mm in

shifts downstream. In the numerical calculation, the local heat flux is calculated as follows :

$$q_{two} = q_{air} + q_{sensible} + q_{latent} = h_{air}(T_w - T_{ad\infty}) + m \cdot C_p \cdot (T_v - T_{aw\infty}) + m \cdot L \quad (21)$$

where m is the mass flux of droplets which attached to the heated flat plate, L is the latent heat of water and h_{air} is the heat transfer coefficient of the air phase in the two-phase flow. The mass loading ratio of water droplets was very small in this experiment, so that the attenuation or enhancement of turbulence does not occur in spite of the existence of the droplets. Therefore, the heat transfer by air in two-phase flow is considered to be same as that in single-phase flow. This means that the increase of heat transfer in two-phase flow mainly depends upon the latent heat transfer due to the evaporation which is proportional to

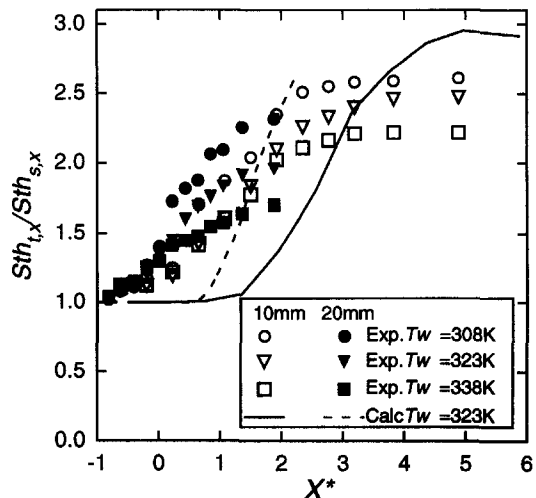


Fig. 14. Ratio of local Stanton number.

the separated shear layer. As another point of view, the turbulent Stokes number for $H = 20$ mm and droplet diameter of $60 \mu\text{m}$, as shown in Fig. 8, became unity around the reattachment region, which means the particles dispersed widely. The diameter of $60 \mu\text{m}$ is the arithmetic diameter in these experiments, so that the droplets of that diameter dominate in the two-phase flow field; see also Fig. 9(a). Thus, the heat transfer enhancement for $H = 20$ mm is larger than that for $H = 10$ mm downstream of the reattachment region in an air-water droplet flow.

CONCLUDING REMARKS

Experimental and numerical studies have been performed on the air-water droplet laden flow behind a backward-facing step to find out the relationship of the flow field and heat transfer, and to examine the possibility of controlling heat transfer in an air-water droplet flow. Flow characteristics are obtained by a two-component PDA for single- and two-phase flows. This work leads to the following conclusions:

It was obvious that the heat transfer in an air-water droplet flow increased considerably over that of a single-phase flow downstream of the reattachment region for both step heights examined. Heat transfer coefficients were enhanced more than twice for single-phase flow in the redeveloping region even for the very low droplet mass loading ratio of 4.1%. The influence of the turbulent motion of the droplets on the heat transfer enhancement appeared downstream of the reattachment region. This enhancement was due to the wider dispersion of the droplets in the separated shear layer which led to higher droplet mass fluxes towards the heated wall, and was well correlated to the turbulent Stokes number which expressed the feature of the energy containing eddies. It was concluded from these results that there was a high potential to control the large heat transfer enhancement by actively varying the Stokes numbers.

Acknowledgements—The authors would like to thank Professor J. K. Eaton of Stanford University for his advice and discussion during his stay as a guest professor at Keio University. We also thank Dr. S. Obi of Keio University for advice on the numerical simulation, and thank Dr. E. Mastorakos for a fruitful discussion, and thank Mr. H. Kawashima, student of Keio University, for performing experiments.

REFERENCES

1. K. Hishida, M. Maeda and S. Ikai, Heat transfer from a flat plate in two-component mist flow, *J. Heat Transfer* **102**, 513–518 (1980).
2. R. Chein and J. N. Chung, Effect of vortex pairing on particle dispersion in turbulent shear flows, *Int. J. Multiphase Flow* **13**(6), 785–802 (1987).
3. R. Chein and J. N. Chung, Simulation of particle dispersion in a two-dimensional mixing layer, *A.I.Ch.E. J.* **34**(6), 946–954 (1988).
4. K. Hishida, A. Ando and M. Maeda, Experiments on particle dispersion in a turbulent mixing layer, *Int. J. Multiphase Flow* **18**(2), 181–194 (1992).
5. P. Bradshaw and F. Y. F. Wong, The reattachment and relaxation of a turbulent shear layer, *J. Fluid Mech.* **52**(1), 113–135 (1972).
6. J. K. Eaton and J. P. Johnston, Turbulent flow reattachment: an experimental study of the flow and structure behind a backward-facing step, Report MD-39, Thermosciences Division, Dept. of Mech. Engng, Stanford University (1980).
7. K. Hishida, H. Wanajo and M. Maeda, Characteristics of gas-solids two-phase flow and heat transfer downstream of the backward-facing step, *Trans. JSME, Ser. B* **51**(467), 2176–2183 (1985) [in Japanese].
8. Y. Hardalupas, A. M. K. P. Taylor and J. H. Whitelaw, Particle dispersion in a vertical round sudden-expansion flow, *Phil. Trans. R. Soc. Lond. A* **341**, 411–442 (1992).
9. K. Kobashi, K. Hishida and M. Maeda, Measurements of fuel injector spray of I.C. engine by FFT based phase Doppler anemometer—an approach to the time series measurements of size and velocity. In *Application of Laser Technique to Fluid Mechanics* (Edited by R. J. Adrian, D. F. G. Durao, F. Durst, M. Maeda and J. H. Whitelaw), pp. 268–287. Springer, Berlin (1990).
10. H. Schlichting, *Boundary Layer Theory* (7th Edn). McGraw-Hill, New York (1979).
11. ASME Performance Test Codes Measurements Uncertainty, ASME (1985).
12. B. E. Launder and D. B. Spalding, The numerical computation of turbulent flows, *Comput. Meth. Appl. Mech. Engng* **3**, 269–289 (1974).
13. P. Bradshaw, T. Cebeci and J. H. Whitelaw, *Engineering Calculation Methods for Turbulent Flow*, p. 54. Academic Press, New York (1981).
14. S. V. Patankar and D. B. Spalding, A calculation procedure for heat, mass and momentum transfer in three-dimensional parabolic flows, *Int. J. Heat Mass Transfer* **15**, 1787–1806 (1972).
15. B. P. Leonard, A stable and accurate convective modelling procedure based on quadratic upstream interpolation, *Comput. Meth. Appl. Mech. Engng* **19**, 59–98 (1979).
16. P. G. Saffman, The lift on a small sphere in a slow shear flow, *J. Fluid Mech.* **22**(2), 385–400 (1965) and Corrigendum, *ibid.* **31**(3), 624 (1968).
17. R. Clift, J. R. Grace and M. E. Weber, *Bubbles, Drops and Particles*. Academic Press, New York (1978).
18. T. Yokomine, A. Shimizu, S. Hasegawa and T. Kawamura, Stochastic simulation of gas-solid suspension flows by means of Reynolds stress turbulent model, *Proceedings of the ASME-JSME Thermal Engineering, Joint Conference*, ASME Book No. 10309B, pp. 81–88 (1991).
19. W. Rodi, A new algebraic relation for calculating the Reynolds stresses, *Mech. Fluid, Z. Angew. Math. Mech.* **56**, T219–T221 (1976).
20. D. M. Driver and H. L. Seegmiller, Features of a reattaching turbulent shear layer in divergent channel flow, *AIAA J.* **23**(2), 163–171 (1985).
21. J. C. Vogel and J. K. Eaton, Combined heat transfer and fluid dynamic measurements downstream of a backward-facing step, *J. Heat Transfer* **107**, 922–929 (1985).
22. T. Ishima, K. Hishida and M. Maeda, Effect of particle residence time on particle dispersion in a plane mixing layer, *J. Fluid Engng* **115**, 751–759 (1993).
23. J. P. Johnston, Internal flows. In *Topics in Applied Physics, Turbulence* (Edited by P. Bradshaw), Vol. 12, pp. 109–165. Springer, Berlin (1978).
24. J. K. Eaton and J. P. Johnston, A review of research on subsonic turbulent flow reattachment, *AIAA J.* **19**(9), 1093–1100 (1981).
25. K. Kudo, H. Taniguchi, T. Kobayashi and T. Fukuchi, Numerical analyses on velocity and temperature fields in the recirculating zone behind a backward-facing step (the influence of Reynolds number), *Trans. JSME, Ser. B* **57**(535), 1071–1076 (1991) [in Japanese].